Advances in Remote Sensing, 2017, 6, 147-159
http://www.scirp.org/journal/ars
ISSN Online: 2169-2688
ISSN Print: 2169-267X

Sentinel-2 MSI Radiometric Characterization and Cross-Calibration with Landsat-8 OLI

Shuang Li[1], Sangram Ganguly[1], Jennifer L. Dungan[2], Weile Wang[3], Ramakrishna R. Nemani[2]

[1]Bay Area Environmental Research Institute (BAERI)/NASA Ames Research Center, Moffett Field, CA, USA
[2]NASA Ames Research Center, Moffett Field, CA, USA
[3]NASA Ames Research Center & University Corporation at Monterey Bay, Moffett Field, CA, USA
Email: shuang.li@nasa.gov

How to cite this paper: Li, S., Ganguly, S., Dungan, J.L., Wang, W.L. and Nemani, R.R. (2017) Sentinel-2 MSI Radiometric Characterization and Cross-Calibration with Landsat-8 OLI. *Advances in Remote Sensing*, **6**, 147-159.
https://doi.org/10.4236/ars.2017.62011

Received: May 16, 2017
Accepted: June 23, 2017
Published: June 26, 2017

Abstract

Near-nadir observations by the Multispectral Instrument (MSI) onboard the Sentinel-2 and the Operational Land Imager (OLI) onboard Landsat 8 were collected during two Simultaneous Nadir Overpasses (SNO). Multispectral images with 10, 20, and 30 m resolution from a spatially uniform area in the Saharan desert were acquired for direct comparison of MSI and OLI Top-Of-Atmosphere (TOA) reflectances. This paper presents an initial radiometric cross-calibration of the 8 corresponding spectral bands of the Sentinel-2 MSI and Landsat 8 OLI sensors. With the well-calibrated Landsat 8 OLI as a reference, the comparison indicates that 6 MSI bands are consistent with OLI within 3% in terms of spectral band adjustment factors B_i. The Near-Infra-Red (NIR) and cirrus bands are exceptions. They yield radiometric differences on the order of 8% and 15% respectively. Cross-calibration results show that the radiometric difference of the 7 corresponding bands are consistent to OLI within 1% or better, except on cirrus band. A pixel-by-pixel match between the MSI and OLI observations for different land covers showed that. This initial study suggests that the red-edge band B8A of MSI can be used to replace the NIR band B08 when conducting vegetation monitoring.

Keywords

Sentinel-2, Landsat 8, Radiometric Calibration, Simultaneous Nadir Observation

1. Introduction

The successful launch of the European Space Agency (ESA) Sentinel-2A on 23 June 2015 with the key instrument MultiSpectral Instrument (MSI) provides an important means to augment Earth-observation capabilities following the legacy of Landsat. After the three-month satellite commissioning campaign, the MSI onboard Sentinel-2 (S-2) is performing very well [1]. By 3 December 2015, the sensor data records have achieved provisional maturity status and have been accessed in level-1C Top-Of-Atmosphere (TOA) reflectance by the remote sensing community worldwide.

Sentinel-2 is an ESA land monitoring mission with two identical satellites that provide high resolution optical imagery. The launch of Sentinel-2B is planned for mid-2016 [2]. After that, the two identical Sentinel-2 satellites (Sentinel-2A and Sentinel-2B) will provide an exceptional revisit capability of 5 days at the equator and 2 - 3 days over mid-latitudes. The twin satellites fly in the same sun-synchronous orbit but phased at 180˚ to each other. The coverage limits are between latitudes 56˚ south and 84˚ north, including all the land surfaces, coastal waters, and Mediterranean Sea. At a nominal equatorial altitude of 786 km, the swath width is 290 km. The wide swath width and high revisit time will support monitoring of changes to vegetation within the growing season. The MSI sensor aboard on Sentinel-2 capitalizes on the technology and the vast experience acquired with SPOT and Landsat over the past decades [3]. The S-2 MSI samples 13 spectral bands covering wavelengths from 0.4 to 2.2 um: four bands at 10 meters, six bands at 20 meters and three bands at 60 meters spatial resolution [4].

In order to meet the requirement for monitoring rapidly changing land processes (e.g. agriculture, wild fire, vegetation phenology, and extreme weather events), the scientists of the NASA Land-Cover and Land-Use Change (LCLUC) program and NASA Multi-source Land Imaging (MuSLI) program have been actively pursuing the synergy of Sentinel-2 and Landsat 8 (L8) data [5]. S-2 MSI and L8 Operational Land Imager (OLI) together make a potent source for higher-rate multispectral observation with global coverage and free and open access. The biggest challenge of using remote sensing data from multiple sources, however, is inter-calibration across different instruments.

This paper explores aspects of the radiometric cross-calibration of the S-2 MSI and L8 OLI sensors based on near-simultaneous imaging of common ground targets in the Saharan desert. Band adjustment factors and linear regression slopes for each band are derived from data at this site. Eight corresponding bands (including aerosol, four visible and near-Infrared bands, cirrus, and two shortwave infrared bands) of MSI are compared with that of OLI in scenes collected during Simultaneous Nadir Overpasses (SNO) and vicarious site.

2. Environmental Data Records (EDRs) from the Multispectral Instrument (MSI)

Sentinel-2 MSI has 13 spectral bands: four visible and near-infrared (VNIR) band with a spatial resolution of 10 m at nadir for optical measurement, four NIR bands (20 m) for vegetation red-edge, two shortwave infrared (SWIR) bands (20 m) for snow, ice, and cloud discrimination, three coarse bands (60 m) in the aerosol, water vapor, and cirrus domain designated for atmospheric correction. The presence of 4 vegetation red-edge bands (B05, B06, B07, B8A) is a unique feature that distinguishes Sentinel-2's MSI from most other multi-spectral satellite sensors. The spectral bands are listed in Table 1. Environmental Data Records (EDRs) derived using these bands are described in detail in [3] and summarized in Table 2.

3. Radiometric Validation of the Sentinel-2 MSI

3.1. Relative Spectral Response (RSR)

Given the similar mission concepts of the Spot and Landsat series sensors (MSS, TM, ETM+, and OLI), the spectral band configuration of the S-2 MSI was designed around the use of Landsat and Spot wavelengths [3]. The S-2 MSI has spectral bands similar to Landsat 8 OLI's, which enable the synergistic use of data from S-2A, S-2B, and Landsat OLI. Figure 1 shows the band-average Relative Spectral Response (RSR) of S-2 MSI together with L8 OLI for matching spectral bands. Since the four red-edge bands (B05, B06, B07, and B8A) and water vapor band (B09) of MSI are new to MSI and have no analogous OLI bands, this study only compares the other eight bands. These are generally comparable to the Landsat 8 OLI bands. The MSI bands for coastal aerosols, cirrus and two SWIR domains follows Landsat OLI sensor for atmospheric correction (upper panel of Figure 1). Compared to the OLI vegetation bands, however, there are significant differences in RSR profiles between corresponding MSI and OLI in three visible bands (Blue, Green, Red) and NIR. The NIR band of MSI is much wider than OLI's (Figure 1).

Table 1. MSI spectral band characteristics.

Band No.	Center λ_{center} (nm)	Spectral width $\Delta\lambda_{center}$ (nm)	Spatial resolution (m)	Driving Environmental Data Records (EDRs)	Radiance sensibility range Lmin[a] < Lref[b] < Lmax[a] (W.m-2.sr-1.µm-1)	SNR[c] Specification (at Lref)
1	443	20	60	Aerosols	16 < 129 < 588	129
2	490	65	10	Blue	11.5 < 128 < 615.5	154
3	560	35	10	Green	6.5 < 128 < 559	168
4	665	30	10	Red	3.5 < 108 < 484	142
5	705	15	20	Vegetation Red-edge	2.5 < 74.5 < 449.5	117
6	740	15	20	Vegetation Red-edge	2 < 68 < 413	89
7	783	20	20	Vegetation Red-edge	1.5 < 67 < 387	105
8a	865	20	20	Vegetation Red-edge	1 < 52.5 < 308	72
8	842	115	10	Near Infrared	1 < 103 < 308	174
9	945	20	60	Water-vapor	0.5 < 9 < 233	114
10	1380	30	60	Cirrus	0.05 < 6 < 45	50
11	1610	90	20	Snow/ice/cloud discrimination	0.5 < 4 < 70	100
12	2190	180	20	Snow/ice/cloud discrimination	0.1 < 1.5 < 24.5	100

[a]The Lmin is the radiance corresponding to the minimum quantized and calibrated data digital number, which is typically "1" or "0" and Lmax is the radiance corresponding to the maximum quantized and calibrated data digital number typically "4095". [b]Lref is the reference radiances. [c]Signal to Noise Ratio (SNR) for the Lref defined for S-2 mission.

Table 2. MSI environmental data records.

Category	Environmental Data Records
Land	Vegetation senescing
	Vegetation carotenoid
	Vegetation browning
	Soil background
	Green peak
	Total chlorophyll in vegetation
	Maximum chlorophyll absorption
	Position of red edge
	Leaf Area Index (LAI)
	Edge of the Near-Infrared (NIR) plateau
	Biomass
	LAI and protein
	Lignin, starch and forest above ground biomass. Snow/ice/cloud separation.
	Assessment of vegetation conditions. Distinction of clay soils for the monitoring of soil erosion. Distinction between live biomass, dead biomass and soil, e.g. for burn scars mapping.
Imagery and Aerosols/Clouds	Water vapor absorption reference
	Atmospheric correction aerosol scattering
	Consolidation of atmospheric corrections/fluorescence baseline
	Retrieval of aerosol load and type
	Detection of thin cirrus for atmospheric correction

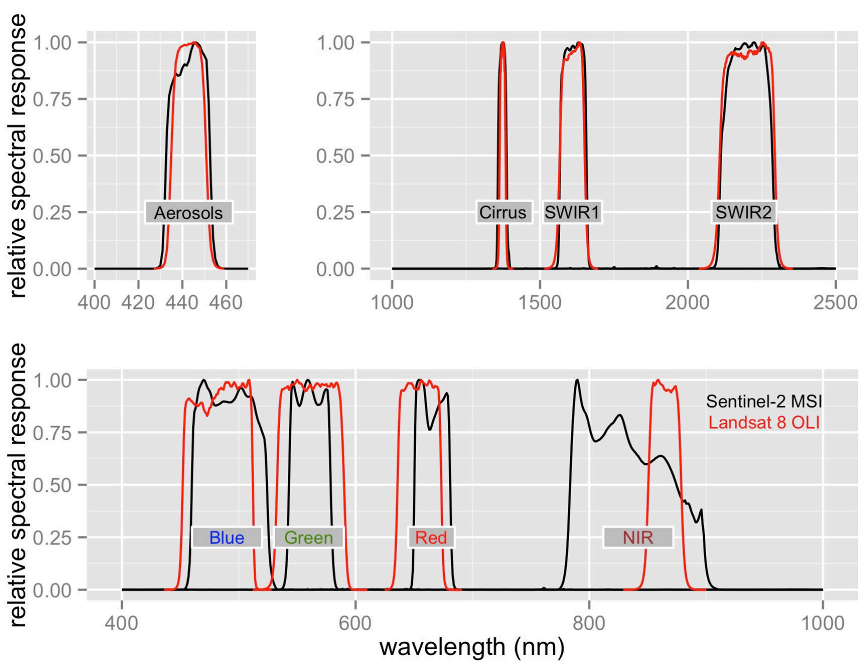

Figure 1. Relative Spectral Response (RSR) of S-2 MSI and L8 OLI.

3.2. S-2 and L8 Image Pairs Selected for Analysis

Level-1C Sentinel-2 MSI images were downloaded from the Scientific Data Hub (https://scihub.copernicus.eu/dhus/#/home). The S-2 Level-1C product is top-of-atmosphere (TOA) reflectance in cartographic geometry. Nearly simultaneous L8 images were ordered using the USGS EROS Science Processing Architecture (ESPA) (http://espa.cr.usgs.gov). ESPA is an on-demand interface that provides Landsat higher-level science data products, including Climate Data Records (TOA reflectance, brightness temperature, cloud masks, and surface reflectance) and spectral indices (e.g. NDVI, EVI, SAVI, and NBR).

Nearly simultaneous observations over the Saharan desert were taken by S-2 MSI and L8 OLI on Dec. 8, 2015 (Table 3). The homogeneous desert area in Figure 2 is used as a pseudo-invariant site in this study for cross-calibration. It located in Algeria, Africa (29˚46'4.19"N, 8˚52'8.80"E) at an elevation of 300 m. This site is at the nadir of Landsat WRS-2 191/039, immediately east of the CEOS reference standard test site Algeria 3 [6] [7]. Sand dunes create variation over much of the scene, but there is a largely spatially homogeneous area over 2.4 by 4.2 km. In order to assess the radiometric characteristics of MSI vegetation bands, an additional MSI and L8 image pair from a forested region in Nigeria is also used in this study (Table 3). The selected MSI and OLI image pairs were unaffected by clouds.

Table 3. Sentinel-2 MSI and Landsat 8 OLI image used for cross-calibration.

Landcover	Sensor	Acquisition Date	Start time	Stop time	Path/Row	Scene ID
Desert	S-2 MSI	Dec. 8, 2015	10:11	10:20	T32RMU (S-2 Tiling Grid)	S2A_OPER_PRD_MSIL1C_PDMC_20151208T190814_R122_ V20151208T102005_20151208T102005
	L8 OLI	Dec. 8, 2015	9:56	9:56	191/039 (WRS2)	LC81910392015342LGN00
Vegetation and coastal water	S2 MSI	Dec. 8, 2015	10:11	10:20	T31NEH (coastal water)	S2A_OPER_PRD_MSIL1C_PDMC_20151208T191315_R122_ V20151208T102005_20151208T102005
	L8 OLI	Dec. 8, 2015	10:02	10:03	191/055 (WRS2)	LC81910552015342LGN00

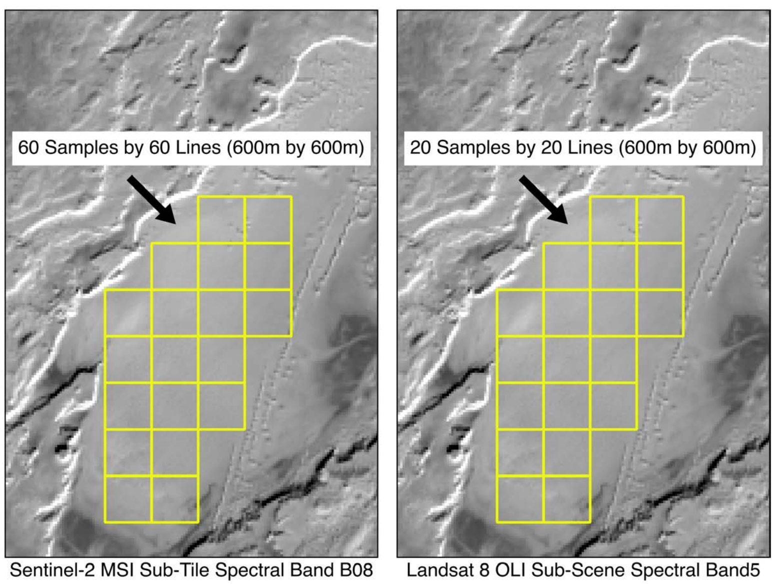

Figure 2. Grid cell analysis scheme illustrated for the desert site, 8 Dec. 2015.

There are 19 grid cells (600 m by 600 m) set up across the site. Each of the contiguous image windows constrains a common ground to both the MSI and OLI image data (**Figure 2**).

SNO events between Sentinel-2 MSI and Landsat 8 OLI satellites occurred at both the Algerian desert and Nigerian forest regions with a time difference within a few minutes on December 8, 2015. The small time difference creates nearly identical viewing conditions (atmosphere, sensor, and solar geometry) and greatly reduces the uncertainties of radiometric bias caused by the surface BRDF and radiation transfer.

3.3. Vicarious Calibration

Vicarious calibration makes use of natural or artificial sites on the Earth's surface for in-flight calibration of satellite sensors [8]-[14]. It has been used successfully for the absolute radiometric calibration of Landsat TM [15]. A reflectance-based approach is one of these vicarious methods. [13] suggested that TOA reflectance comparisons have the potential to yield the best possible calibration comparisons between two sensors with near simultaneous nadir data acquisitions, because, 1) the cosine effect of different solar zenith angles was removed and 2) proper compensation for the exo-atmospheric solar irradiance was supplied.

The key radiometric equations for cross-calibration of Landsat satellites have been developed and applied by [15] [16]. Following these equations, sensor MSI responsivity $G_{i\mathrm{MSI}}$ in spectral band *i* is given by:

$$G_{i\mathrm{MSI}} = M_i G_{i\mathrm{OLI}} \tag{1}$$

where M_i is the slope of the linear equation that characterizes MSI responsivity as a function of $G_{i\mathrm{OLI}}$. Here, $G_{i\mathrm{OLI}}$ is OLI responsivity in spectral band *i*, this leads to

$$M_i = \frac{G_{i\mathrm{MSI}}}{G_{i\mathrm{OLI}}} = B_i \left(\frac{E_{0i\cos\theta\mathrm{OLI}}}{E_{0i\cos\theta\mathrm{MSI}}} \right) \left(\frac{\Delta Q_{i\mathrm{MSI}}}{\Delta Q_{i\mathrm{OLI}}} \right) \tag{2}$$

Original definitions of the variables in Equation (2) can be found in [15] [16] [17], where $\Delta Q_{i\mathrm{MSI}}$ and $\Delta Q_{i\mathrm{OLI}}$ are bias-corrected image values, $E_{0i\cos\theta\mathrm{MSI}}$ and $E_{0i\cos\theta\mathrm{OLI}}$ are the exo-atmospheric solar irradiance (in Watts/(m^2·μm)), two θ are the solar zenith angles of MSI and OLI. Equation (2) is developed for the cross-calibration start from raw data (or level 0).

The main part of Equation (2) is the spectral band adjustment factor, $B_i = \rho^*_{i\mathrm{OLI}} / \rho^*_{i\mathrm{MSI}}$. Its uncertainty is directly proportional to the uncertainty in the cross calibration [17].

In this study, bi-directional reflectance effects are not expected to be significant since the selected uniform areas have near-nadir viewing geometry and the sun-angle differences between the image pairs are small. In addition, small misregistration is not expected to have an impact on the result because of the degree of spatial homogeneiety of the test area.

4. Results

Spectral Band Adjustment Factors

The spectral band adjustment factors B_i were computed from pixels in the grid cells from the image pair over the desert site (**Figure 3**). The spectral band difference effect less than 3%, except in NIR and cirrus bands. The B_i value for NIR is on the order of 8%, which is mostly caused by the difference of spectral profile between MSI and OLI. The B_i value for cirrus band is even larger, on the order of 15%, though the spectral profile of cirrus of MSI is perfectly matched with OLI's (**Figure 1** & **Figure 3**).

The TOA reflectance of the grid cells (**Figure 2**) are used to explore the radiometric calibration factors for the corresponding bands between MSI and OLI. The mean values across the cells were extracted and plotted to estimate the slopes M_i (Equation (1) & (2)).

Figure 4 shows plot for the eight corresponding bands (MSI against OLI), and **Table 4** lists the slope results. The scatter plot of cirrus band is placed at the bottom right corner of **Figure 4** due to its scale issue.

Figure 5 together with **Table 4** present the derived slopes M_i and their correlation coefficients. On the left panel of **Figure 5**, the measurements of MSI are almost always higher than that of OLI in the bands of aerosols, blue, red, and SWIR1, where the derived slope of SWIR1 is significantly lower than the others, only 0.497. The measurements of MSI in the cirrus and NIR band, however, are much lower than the OLI's. There is more scatter in the cirrus band, averaging approximately 0.377 in terms of slope and 0.413 in terms of R-squared. The slope values M_i derived from the Saharan calibration site show that cross-calibration is successful in the aerosol, blue, green, and SWIR2 bands. **Figure 4** & **Figure 5**, **Table 4** also clearly shows the issue in the NIR band between the two sensors.

Figure 6 presents the calibration results from **Table 4** in terms of percentage of difference compared with Landsat OLI measurements during the SNO event. The results in **Figure 6** show that almost all the differences are well within the 1% range, except in the cirrus band where the difference after calibration is around 2.5%. The calibrated MSI measurement in SWIR2 is a little bit off the

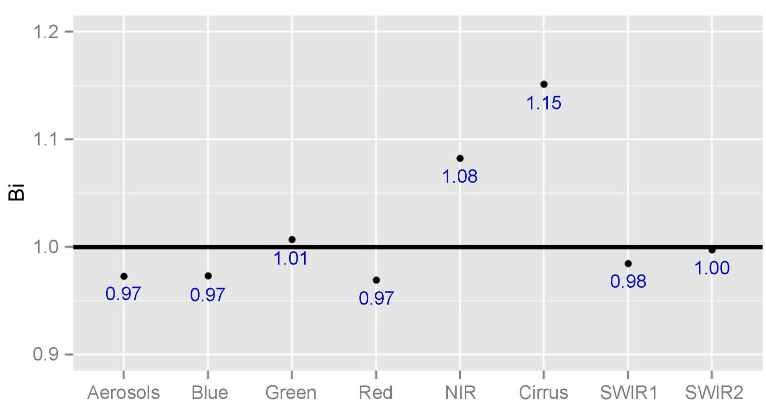

Figure 3. Comparison of spectral band adjustment factors B_i.

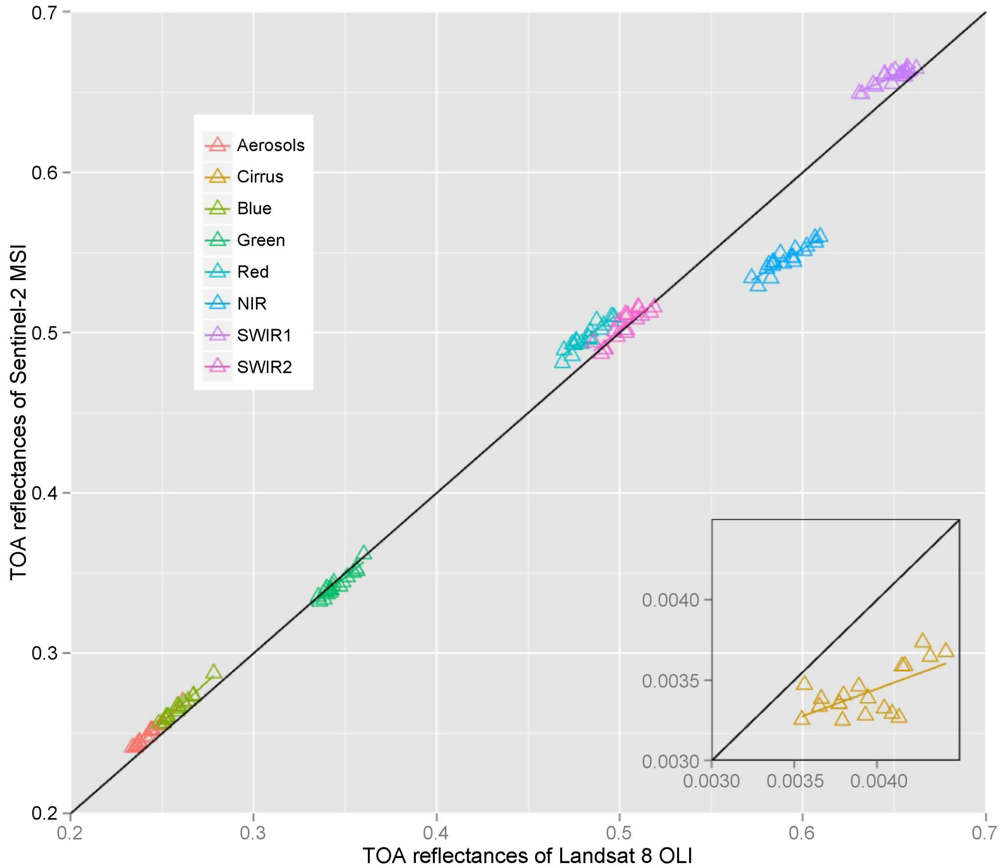

Figure 4. Plot of grid-cell TOA reflectances of MSI and OLI. The subplot at the lower right corner is for the cirrus band.

Table 4. Linear fit results corresponding to the plots shown in Figure 4 & Figure 5.

Spectral band	M_i (Slope)	Intercept	R-squared
Aerosols	1.052	−0.006	0.988
Cirrus	0.377	0.002	0.413
Blue	1.031	−0.001	0.985
Green	0.956	0.013	0.921
Red	0.860	0.083	0.877
NIR	0.707	0.128	0.853
SWIR1	0.497	0.337	0.794
SWIR2	0.918	0.043	0.771

referenced OLI value. The calibration result in the NIR band is better than one might expect given that the spectral profiles of the two sensors are significantly different in this band.

In order to further assess the magnitude of the VNIR band difference effect between Sentinel-2 MSI and Landsat OLI, spatial statistics were computed across a variety of land covers: coastal water, urban, natural forest, and desert. Statistics of TOA reflectance of the two sensors are also extracted from the SNO image pair (Table 3). In general, the SNO scene imaged by the two sensors is assumed

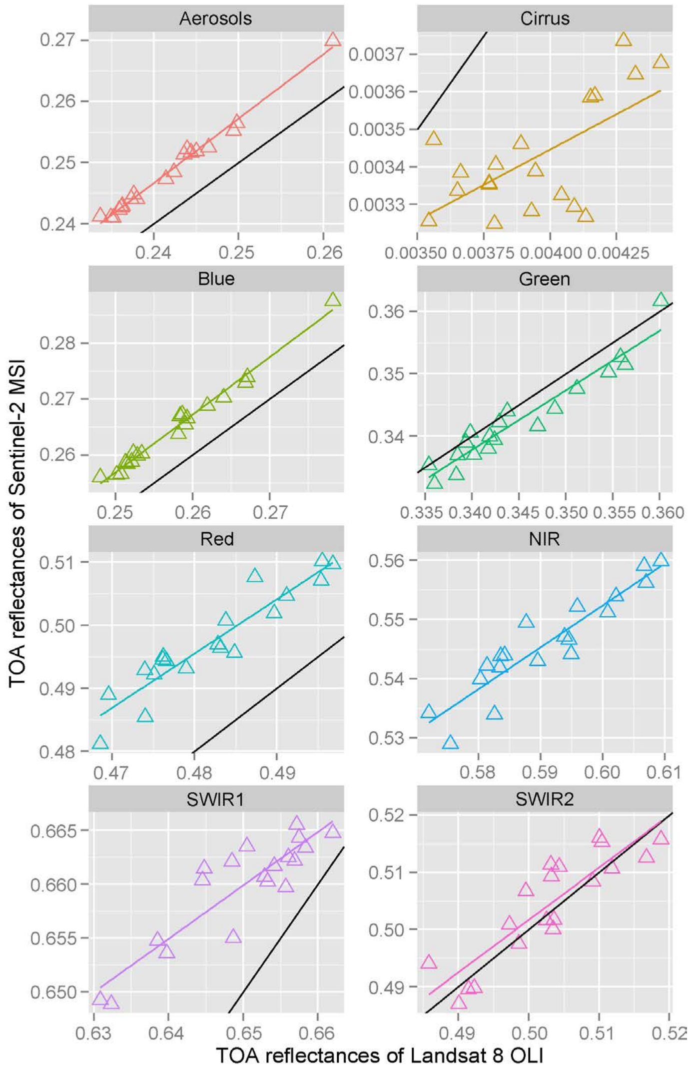

Figure 5. Detailed plots from **Figure 4** with best fit lines for each band (black lines are 1:1).

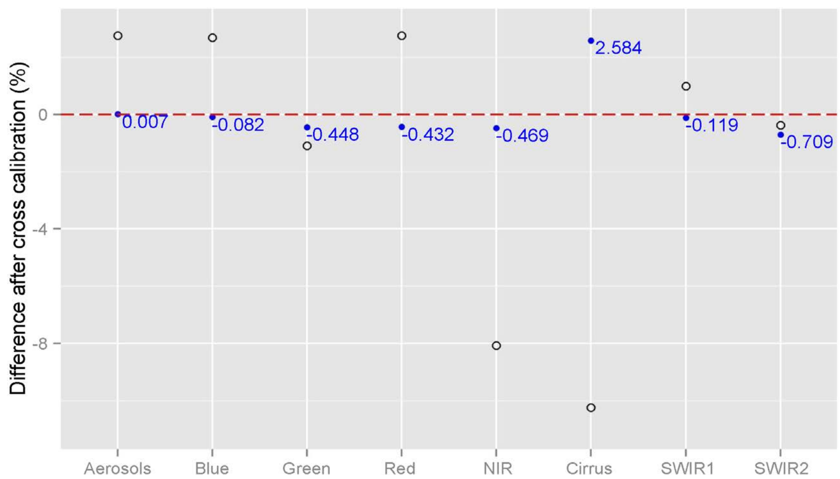

Figure 6. Cross-calibration results in eight spectral bands. Open circles denote measurements from Sentinel-2 MSI before M_i were applied, closed circles denote the differences after M_i were applied.

to be with the same sun-angle and off-nadir viewing geometry. Figure 7 plots the TOA reflectance change over different land surface. The comparison for the three visible bands (Blue, Green, and Red) yield small differences with dark surface (e.g. coastal water and natural vegetation), while the spectral band difference effects are larger over bright surface objects (e.g. heavy developed areas and desert). NIR band, however, shows significant spectral differences over variety of surfaces, with except of coastal water (Figure 7). This abnormal of NIR domain may be caused by the differences in NIR RSR profiles between the two sensors (Figure 1 & Figure 7).

5. Discussion

The four VNIR bands have wide applications in remote sensing and imaging spectroscopy [18]. The cross-calibration results show that the blue channel yields the best adjustment. The difference after cross-calibration is 0.082% compared to the reference blue channel of L8 OLI. The difference after cross-calibration in the Green, Red, and NIR are on the order of 0.4%. In comparison with the significant difference of the RSRs of NIR bands in MSI and OLI, the cross-calibration performance of the MSI NIR band is promising.

The NIR band is well known to be critical to the biophysical factors of vegetation monitoring. Figure 8 shows a direct comparison of NIR bands of Sentinel-2 and Landsat. There are significant differences in relative spectral response profiles between Sentinel-2 MSI and Landsat sensors (ETM+ and OLI) in the NIR. The design of NIR band of Landsat 7 ETM+ followed the Landsat TM series, which spans 760 - 900 nm (Figure 8). The NIR band of L8 OLI avoids heavy water vapor contamination, using a narrow spectrum 850 - 880 nm. The RSR of the NIR band of MSI, however, is more complex than that of L8 OLI. Fortunately, S2 MSI provides four additional red-edge bands (B05, B06, B07, and B8A),

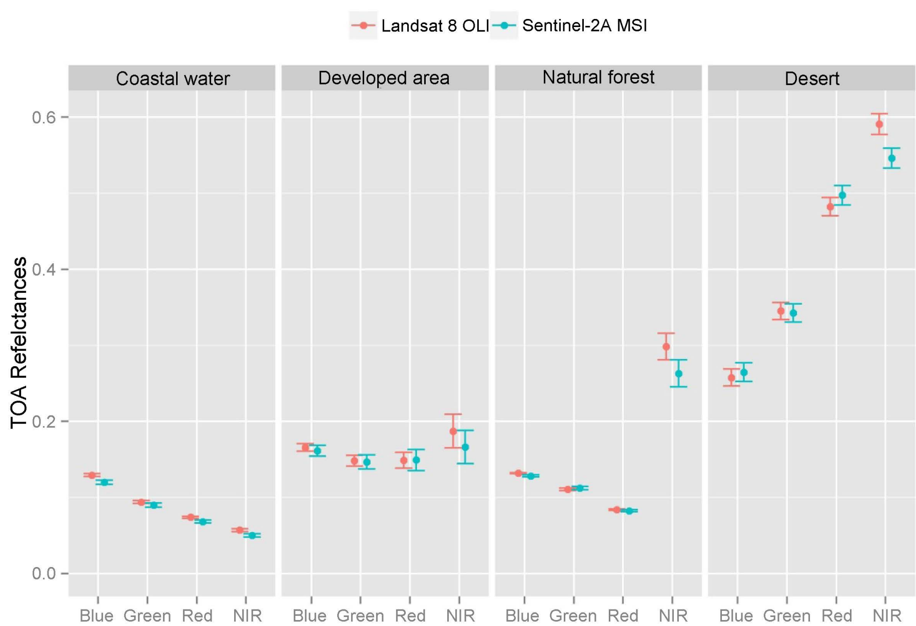

Figure 7. Comparison of TOA reflectance across typical surface covers.

though the resolution is 20 m. The RSR of MSI's red-edge band B8A is similar to OLI's NIR (Figure 8). Both narrow bands are centered at 865 nm.

$$\mathrm{NDVI} = \frac{\mathrm{NIR} - \mathrm{Red}}{\mathrm{NIR} + \mathrm{Red}} \tag{3}$$

Using alternative band combinations, we calculated Normalized Difference Vegetation Indices (NDVI) for L8 OLI and S-2 MSI (Equation (3)) from the Nigerian scene which is covered by natural forest with a relatively homogenous texture. Table 5 shows the performance of MSI B8A is much better than B08. The NDVI calculated using the B8A and B04 combination shows a larger data range. Its mean value is close to the OLI's NDVI value. This result suggests that B8A of MSI removes heavy water vapor influence yet is still sensitive enough for vegetation detection.

This result raises concerns about the MSI NIR band in data harmonization between S-2 MSI and L8 OLI. It also suggests that using B8A is a good option when calculating vegetation indices (e.g. NDVI).

6. Conclusions

A first cross-calibration of S-2 MSI and L8 OLI has been presented in this study. Image pairs captured during an SNO event are used to perform the radiometric cross-calibration. Nearly coincident data acquisitions over common targets make it possible to use image data from the well-calibrated L8 OLI to calibrate

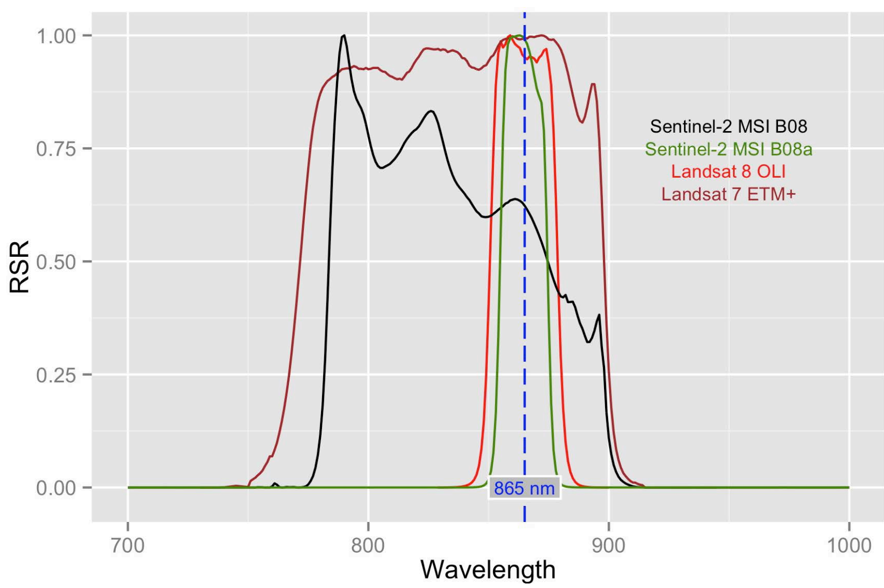

Figure 8. Comparison of NIR Relative Spectral Response (RSR) profiles.

Table 5. Statistics of NDVI computed with varied band combinations.

Sensor	NDVI	Min	max	mean	majority	std
Sentinel-2 MSI	(B08 – B04)/(B08 + B04)	0.377	0.611	0.522	0.500	0.025
Sentinel-2 MSI	(B8A – B04)/(B8A + B04)	0.472	0.648	0.573	0.600	0.021
Landsat OLI	(b5 – b4)/(b5 + b4)	0.499	0.626	0.560	0.556	0.020

S-2 MSI in analogous spectral bands. Given that Landsat 8 OLI is well-understood radiometrically [5], cross-calibration between the L8 OLI and other multispectral land imaging sensors (e.g. Landsat MSS, TM, and ETM+) can be considered in future studies.

During the development of Landsat 8 and S-2A, the two agencies (ESA and NASA) had joined calibration scientists to ensure that S-2 MSI and Landsat 8 OLI data offer compatible data products, thereby bringing greater benefits to the remote sensing communities of Earth's land and coastal zones. The preliminary results from this study indicate that the overall performance of MSI is a promising addition to the longest operating Earth Observation mission (Landsat). It will significantly augment the Landsat legacy and future Landsat missions (eg. Landsat 9, 10 and beyond).

Acknowledgements

The work described in this paper was performed under NASA contract ARC-CREST, #NNX12AD05A.

References

[1] ESA (2015) Mission Status Reports. https://sentinels.copernicus.eu/web/sentinel/missions/sentinel-2/mission-status

[2] ESA (2016) Sentinel-2 Mission. https://sentinels.copernicus.eu/web/sentinel/missions/sentinel-2

[3] Drusch, M., Del Bello, U., Carlier, S., Colin, O., Fernandez, V., Gascon, F., Hersch, B., Isola, C., Laberinti, P., Martimort, P., Meygret, A., Spoto, F., Sy, O., Marchese, F. and Bargellini, P. (2012) Sentinel-2: ESA's Optical High-Resolution Mission for GMES Operational Services. *Remote Sensing of Environment*, **120**, 25-36.

[4] Malenovský, Z., Rott, H., Cihlar, J., Schaepman, M.E., García-Santos, G., Fernandes, R. and Berger, M. (2012) Sentinels for Science: Potential of Sentinel-1, -2, and -3 Missions for Scientific Observations of Ocean, Cryosphere, and Land. *Remote Sensing of Environment*, **120**, 91-101.

[5] Roy, D.P., Wulder, M.A., Loveland, T.R., Woodcock, C.E., Allen, R.G., Anderson, M.C., Helder, D., Irons, J.R., Johnson, D.M., Kennedy, R., Scambos, T.A., Schaaf, C.B., Schott, J.R., Sheng, Y., Vermote, E.F., Belward, A.S., Bindschadler, R., Cohen, W.B., Gao, F., Hipple, J.D., Hostert, P., Huntington, J., Justice, C.O., Kilic, A., Kovalskyy, V., Lee, Z.P., Lymburner, L., Masek, J.G., McCorkel, J., Shuai, Y., Trezza, R., Vogelmann, J., Wynne, R.H. and Zhu, Z. (2014) Landsat-8: Science and Product Vision for Terrestrial Global Change Research. *Remote Sensing of Environment*, **145**, 154-172.

[6] Chander, G., Christopherson, J.B., Stensaas, G.L. and Teillet, P.M. (2007) Online Catalogue of World-Wide Test Sites for the Post-Launch Characterization and Calibration of Optical Sensors. *Proceedings of the International Astronautical Federation-58th International Astronautical Congress*, Hyderabad, 24-28 September 2007.

[7] Kotchenova, S.Y., Vermote, E.F., Matarrese, R. and Klemm, F.J. (2006) Validation of a Vector Version of the 6S Radiative Transfer Code for Atmospheric Correction of Satellite Data. Part I: Path Radiance. *Applied Optics*, **45**, 6762-6774. https://doi.org/10.1364/AO.45.006762

[8] Biggar, S.F., Thome, K.J. and Wisniewski, W. (2003) Vicarious Radiometric Cali-

bration of EO-1 Sensors by Reference to High-Reflectance Ground Targets. *IEEE Transactions on Geoscience and Remote Sensing*, **41**, 1174-1179. https://doi.org/10.1109/TGRS.2003.813211

[9] Cao, C., Weinreb, M. and Xu, H. (2004) Predicting Simultaneous Nadir Overpasses among Polar-Orbiting Meteorological Satellites for the Intersatellite Calibration of Radiometers. *Journal of Atmospheric and Oceanic Technology*, **21**, 537-542. https://doi.org/10.1175/1520-0426(2004)021<0537:PSNOAP>2.0.CO;2

[10] Cao, C., Xiong, J., Blonski, S., Liu, Q., Uprety, S., Shao, X., Bai, Y. and Weng, F. (2013) Suomi NPP VIIRS Sensor Data Record Verification, Validation, and Long-Term Performance Monitoring. *Journal of Geophysical Research*: *Atmospheres*, **118**, 664-678. https://doi.org/10.1002/2013jd020418

[11] Koepke, P. (1982) Vicarious Satellite Calibration in the Solar Spectral Range by Means of Calculated Radiances and Its Application to Meteosat. *Applied Optics*, **21**, 2845-2854. https://doi.org/10.1364/AO.21.002845

[12] Thome, K.J. (2001) Absolute Radiometric Calibration of Landsat 7 ETM+ Using the Reflectance-Based Method. *Remote Sensing of Environment*, **78**, 27-38.

[13] Thome, K.J., Biggar, S.F. and Wisniewski, W. (2003) Cross Comparison of EO-1 Sensors and Other Earth Resources Sensors to Landsat-7 ETM+ Using Railroad Valley Playa. *IEEE Transactions on Geoscience and Remote Sensing*, **41**, 1180-1188. https://doi.org/10.1109/TGRS.2003.813210

[14] Thome, K.J. (2004) In-Flight Intersensor Radiometric Calibration Using Vicarious Approaches. In: Morain, S.A. and Budge, A.M., Eds., *Post-Launch Calibration of Satellite Sensors*, Taylor and Francis, London, 95-102. https://doi.org/10.1201/9780203026830.ch11

[15] Teillet, P.M., Barker, J., Markham, B.L., Irish, R.R., Fedosejevs, G. and Storey, J.C. (2001) Radiometric Cross-Calibration of the Landsat-7 ETM+ and Landsat-5 TM Sensors Based on Tandem Data Sets. *Remote Sensing of Environment*, **78**, 39-54.

[16] Teillet, P.M., Fedosejevs, G., Thome, K.J. and Barker, J.L. (2007) Impacts of Spectral Band Difference Effects on Radiometric Cross-Calibration between Satellite Sensors in the Solar-Reflective Spectral Domain. *Remote Sensing of Environment*, **110**, 393-409.

[17] Teillet, P.M., Markham, B.L. and Irish, R. (2006) Landsat Cross-Calibration Based on Near Simultaneous Imaging of Common Ground Targets. *Remote Sensing of Environment*, **102**, 264-270.

[18] Ben-dor, E., Inbar, Y. and Chen, Y. (1997) Reflectance Spectra of Organic Matter in the Visible Near-Infrared and Short Wave Infrared Region (400 - 2500 nm) during a Controlled Decomposition Process. *Remote Sensing of Environment*, **61**, 1-15.